Using short-time creep relaxation effect to decrease the residual stress in the bonded compliant seal of planar solid oxide fuel cell — A finite element simulation

Yu-Cai Zhang [a], Wenchun Jiang [a,b], Shan-Tung Tu [a,*], Jian-Feng Wen [a], Wanchuck Woo [c]

[a] Key Laboratory of Pressure Systems and Safety (MOE), School of Mechanical and Power Engineering, East China University of Science and Technology, Shanghai 200237, PR China
[b] State Key Laboratory of Heavy Oil Processing, College of Chemical Engineering, China University of Petroleum(East China), Qingdao 266555, PR China
[c] Neutron Science Division, Korea Atomic Energy Research Institute, Daejeon 305-353, Republic of South Korea

HIGHLIGHTS

- A holding time at 600 °C during brazing is designed to reduce the residual stress.
- The holding time has been determined by a thermal-elasto-plastic-creep simulation.
- The simplified method for brazing simulation can underestimate the residual stress..
- The simulation method is verified by neutron diffraction experiment.

ARTICLE INFO

ABSTRACT

Bonded compliant seal is a new sealing design for planar solid oxide fuel cell. During brazing, large residual stresses are generated which have a great effect on failure of the brazing connection. Therefore, how to decrease the residual stresses is a critical issue for structure integrity. This paper presents a study on decreasing residual stresses by using short-time creep relaxation effect. A sequential-coupled calculation model is developed based on finite element method. The brazing temperature field is firstly obtained by simulating the convection and radiation heating, and then the residual stress is calculated by a thermal-elasto-plastic-creep model. The calculated results are verified by neutron diffraction measurements. During cooling, a short holding time at 600 °C is designed to relax the residual stress by creep effect. The results show that this effect has a remarkable impact on decreasing the residual stress. The stresses in cell, Ag—CuO and foil have been reduced by about 26.9%, 13.6% and 22.1%, respectively, as the holding time increases up to 40 h. When the holding time exceeds 40 h, the residual stresses remain almost unchanged. It is thus suggested that the holding time should be reasonably determined to allow sufficient stress relaxation.

1. Introduction

Planar solid oxide fuel cell (SOFC) converts the chemical energy to electricity directly through electro-chemical reactions. It has a higher efficiency than the traditional combustion power generator [1,2], and has been a research focus in recent years [3—5]. Since SOFC uses gas as the fuel and works at elevated temperature, a good sealing performance is required to prevent the leakage. The traditional sealing methods, such as rigid sealing and compressive sealing, cannot meet the requirements of long-term operation at elevated temperature. This has been the main obstacle that prevents the full commercialization of SOFC. In recent years, a new sealing method, which is named bonded compliant seal (BCS), has been developed by Weil et al. [6]. It incorporates the advantages of both the rigid and compressive sealing methods, and uses a thin foil metal to bond to the window frame and cell, which can mitigate or trap some thermal stress produced in the BCS structure. It is proved that this sealing method is able to accommodate a significant degree of thermal mismatch strain between the metallic support structure and the ceramic cell via elastic and plasticity deformations of the foil [7]. The ability to accommodate large thermal strain mismatches can reduce the requirements of material mechanical performances. Consequently, the BCS expands the list of

* Corresponding author. Tel./fax: +86 (0)21 64253425.
E-mail address: sttu@ecust.edu.cn (S.-T. Tu).

candidate materials used in SOFC and has a good application prospect.

However, the bonding temperature is very high ($\sim 1050\,^\circ$C) and can introduce large residual stresses caused by the dissimilar materials, geometry discontinuity and temperature gradient, which can have a great effect on service life of creep, stress corrosion cracking and/or fatigue in the long time operation [8]. Obtaining the stress distribution in BCS structure is the first step to understand these failures, which can help to get a reliable joint and extend the service life. Typical means to measure the residual stress are X-ray diffraction, neutron diffraction, etc. X-ray diffraction has a limited penetration depth on the metal, and the measured values are easily affected by the surface condition. The advantage of neutron diffraction is that it can measure the through-thickness stress, but the test cost is high. An effective approach to solve this problem is to use the finite element method (FEM), which can analyze the stress magnitude and distribution in such a complex BCS structure [9–12]. Weil et al. [9] investigated the thermal stress in the BCS structure by three-dimensional FEM, and found that the elastic and plastic deformations of the foil were able to accommodate a significant degree of the thermal stress in the structure. Jiang et al. [10–12] studied the residual stress in BCS structure by FEM, and the effects of brazing parameters on residual stress have been discussed. It is proposed that the thickness of foil should not exceed 80 μm. The above calculation method assumed that the stress at brazing temperature was free, and the stress was calculated during the cooling only, ignoring the process of heating and holding temperature, which may lead to some errors. Therefore in this paper, the brazing temperature through the whole process is firstly calculated by simulating the heat conduction, convection and radiation, and then the temperature field is incorporated into the stress calculation model, aiming to get a more realistic stress distribution.

Reducing the residual stress is important to ensure the structure integrity. The measures such as post-welding heat treatment (PWHT) and slow cooling can be very beneficial to alleviate the residual stress. But PWHT can easily lead to significant deformation because the BCS structure is very thin, and slow cooling is likely to induce the alloy sensitization and decrease the corrosion resistance. We hence propose a new method using short-time creep effect to decrease the residual stress, which is critically examined by using finite element method.

2. Thermo-mechanical finite element analysis

2.1. Finite element model

Fig. 1 shows the cross-section of the BCS structure. Dissimilar materials are assumed to be perfectly bonded at interfaces. The thickness and material of each component are listed in Table 1 [7]. The temperature field and residual stress are simulated by a commercial code ABAQUS. Because the BCS structure displays fourfold
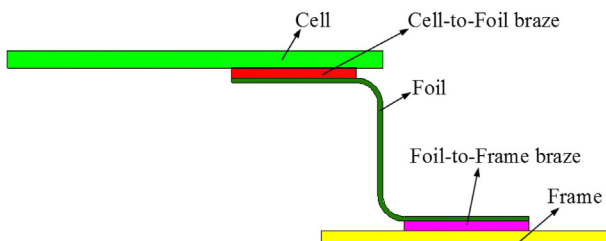
Table 1
Dimensions and materials for the components of BCS structure.

Component	Cell	Cell-to-foil braze	Foil	Foil-to-frame braze	Frame
Thickness (μm)	600	100	50	100	500
Material	Ni–YSZ/YSZ	Ag–CuO	FeCrAlY	BNi-2	Haynes 214

symmetry, one quarter of the model is built. The finite element mesh is shown in Fig. 2. The element types of temperature and stress calculation are DC3D8 and C3D8R, respectively. There are totally 66,798 elements and 90,297 nodes in the 3D model. In order to verify the mesh independence on the calculation result, another two finite element models are built, which are meshed by 40,318 and 81,102 elements, respectively.

2.2. Boundary conditions

Due to the symmetry of BCS structure, two cross-sections of the 3D model are applied on the symmetric boundary conditions. And all the nodes on the bottom face of the window frame are constrained in Z-direction.

2.3. Temperature field simulation

The BCS structure of the planar SOFC is brazed in the vacuum furnace. At first the stacking is heated to 850 °C at 10 °C min^{-1} and the temperature is held for about 40 min to volatilize the binder. Then it is heated to the brazing temperature of 1050 °C and held for about 25 min. At the cooling process, the assembly is firstly cooled to 600 °C, and then held for a period of time at the furnace, and finally cooled to the ambient temperature in the furnace filled with nitrogen [13], as marked (1)–(7) in Fig. 3. At high temperature, an excessively long holding time will bring the corrosion pits in the joint [14]. Therefore, we design another holding temperature at 600 °C (stage (6) in Fig. 3), which is expected to decrease some residual stress by short-time creep effect without causing sensitization of the alloys FeCrAlY and Haynes 214 [15]. The temperature through the whole brazing process is modeled. The thermal analysis involves the natural heat convection, the heat radiation, as well as the thermal conduction between the components and ambient. The results from this calculation method will be closer to those in the actual situation than the simplified method in Refs. [9–12].
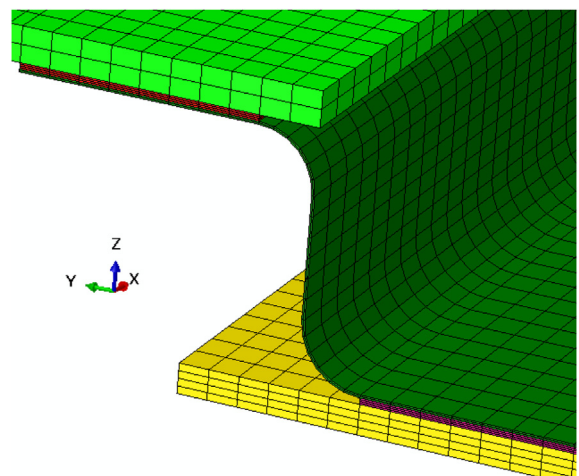

Fig. 1. Cross-section of the BCS structure.
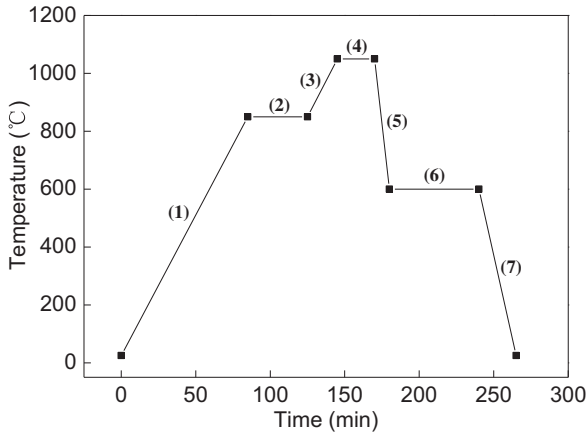

Fig. 2. Finite element meshing.

Fig. 3. Temperature curve of brazing.

The heat conduction between the components and the ambient is calculated by:

$$s = -\left(\rho C \frac{\partial T}{\partial t} + \nabla(K\nabla T)\right) \tag{1}$$

where s is the volume of the heat source, ρ the material density, C the specific heat, T the temperature, t the time, and K the conductivity.

The heat convection is calculated through:

$$\Phi = hA\left(t_{\mathrm{w}} - t_{\mathrm{f}}\right) \tag{2}$$

where Φ is the heat transfer in unit time, h the convective heat transfer coefficient, A the contacting area, t_{w} the temperature of solid surface, and t_{f} the temperature of fluid.

The radiation is calculated by:

$$q = \varepsilon \omega A_1 F_{12}\left((T_1 + 273.15)^4 - (T_2 + 273.15)^4\right) \tag{3}$$

where q is the rate of heat flow, ε the emissivity, the value fall in between 0 and 1, ω the Stefan–Boltzmann constant, A_1 the area of radiation surface 1, F_{12} the shape factor from radiation surface 1 to radiation surface 2, T_1 the temperature of radiation surface 1, and T_2 the radiation surface 2.

In this thermal analysis, the structure is in a vacuum state at the stage (1)–(6), so the heat convection only happened at stage (7). h is a non-physical property parameter and related with the ambient. The size of brazed structure is small compared to the space of furnace, so the convective heat transfer coefficient h can be considered as a constant, $h = 10\ \mathrm{W\,m^{-2}\,K^{-1}}$ in the present paper. In the furnace, $\varepsilon = 0.8$, $\omega = 5.67 \times 10^{-8}\ \mathrm{W\,m^{-2}\,K^{-4}}$, $F_{12} = 1$, and the other thermal properties are summarized in Table 2 [16]. The temperature history of all the nodes is stored in a file for the subsequent residual stress calculation.

Table 2
Thermal properties applied in the FE model.

Material	Ni–YSZ/YSZ	Ag–CuO	FeCrAlY	BNi-2	Haynes 214
Density ($\mathrm{kg\,m^{-3}}$)	3030	10,490	7500	7880	8050
C ($\mathrm{J\,kg^{-1}\,K^{-1}}$)	595	236	458	458	579
K ($\mathrm{W\,m^{-1}\,K^{-1}}$)	5.84	429	186	93.2	22.1

2.4. Residual stress calculation

The residual stress is calculated by using the temperature distribution obtained from the thermal analysis. In this study, the materials are assumed isotropic and temperature dependent. The total strain rate can be decomposed into elastic strain, plastic strain, thermal strain and creep strain. The material of cell is ceramic, so only elastic strain, thermal strain and creep strain are considered. The yield stresses of the other materials are followed by Von Mises criterion. The material properties used in the calculation are elastic modulus, coefficient of thermal expansion, yield strength and Poisson's ratio, as presented in Fig. 4 [9,17–22].

Since the size of the model is small, the temperature changes evidently and the cooling time is relatively short. So it is assumed the creep only occurs in the holding period at 600 °C as shown in Fig. 3. The creep deformation is assumed to follow Norton power law [23–25].

$$\dot{\varepsilon}_{\mathrm{c}} = A\exp(-Q_c/RT)\sigma^n = B\sigma^n \tag{4}$$

in which $\dot{\varepsilon}_{\mathrm{c}}$ is the creep strain rate, A, n are the material constants, Q_c the activation energy, R the Boltzmann gas constant, σ the stress, T the absolute temperature, and $B = A\exp(-Q_c/RT)$.

The creep parameters used in the simulation are listed in Table 3, which are obtained from Refs. [26–28] and fitted from the experimental data [29–31].

3. Experimental verification method

3.1. Sample preparation

In the BCS structure, because the component thickness is very thin, and thus it is very difficult to measure the through-thickness stress. In order to verify the present calculation method, a simplified model with enlarged thickness is built, and the residual stress through the thickness is measured by neutron diffraction. Fig. 5(a) shows a sketching of the simplified model. Two plates with the same dimensions are lap jointed by vacuum brazing in a furnace. The plate length, width and thickness are 100 mm, 30 mm and 4 mm, respectively. Their materials are FeCrAlY and Inconel alloy C276, respectively. The lap length is 10 mm, and the filler metal thickness is 70 μm. In order to avoid the model deformation, a support plate shown in Fig. 5(a) is used but it is not brazed to the sample. Before assembling, each plate was degreased, acid etched, detergent washed and dried. Then the assembly was put in a vacuum furnace and heated according to the thermal history of the processing as shown in Fig. 3.

3.2. Neutron diffraction (ND) measurement

After the sample preparation, the residual stress was measured by neutron diffraction method, as shown in Fig. 5(b). It was performed at Korea Atomic Energy Research Institute [32]. This method is based on the Bragg's law:

$$N\lambda = 2d\sin\theta \tag{5}$$

where d is the lattice spacing, N an integer and 2θ the diffraction angle. The strain (ε) is calculated by measuring the scattering angle (θ) of a material under stress and the scattering angle (θ_0) of the same material in a free of stressed state. Thus, the ε is given by

$$\varepsilon = \frac{\Delta d}{d} = -(\theta - \theta_0)\cot\theta \tag{6}$$

The three principal stresses can be calculated by using the generalized Hook's law. It converts the elastic strains ($\varepsilon_{xx},\ \varepsilon_{yy},\ \varepsilon_{zz}$) to
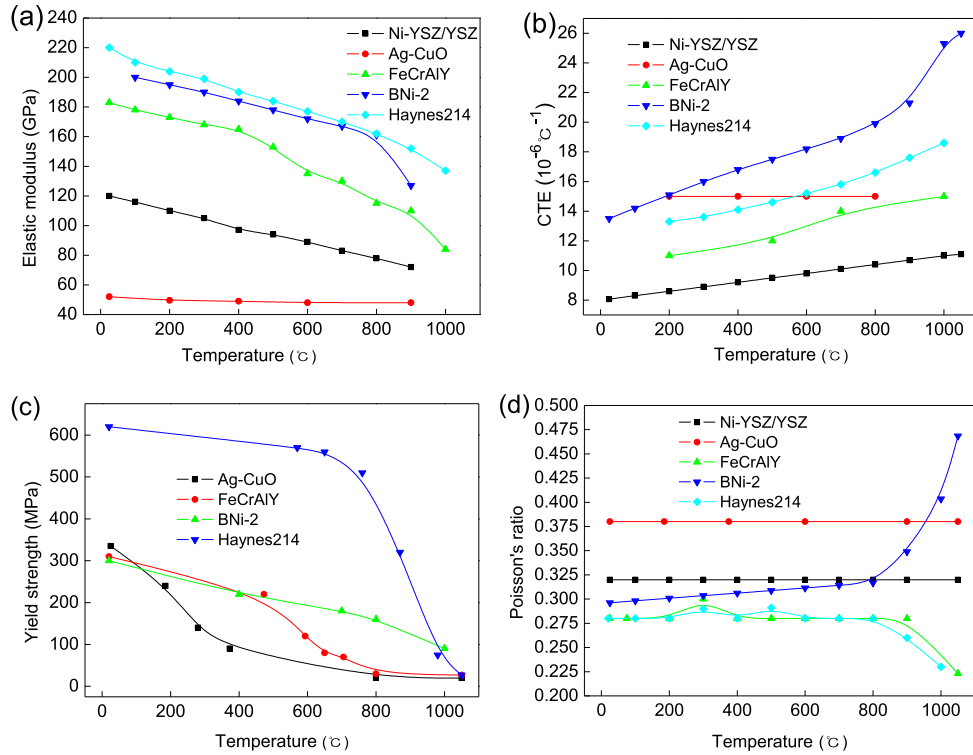
Fig. 4. Mechanical properties: (a) elastic modulus, (b) coefficient of thermal expansion, (c) yield strength, and (d) Poisson's ratio.

Table 3
Creep parameters applied in the FE model (600 °C).

Material	Ni−YSZ/YSZ [26]	Ag−CuO [29]	FeCrAlY [27]	BNi-2 [28]	Haynes 214 [30,31]
B (MPa^{-n} s^{-1})	7.33×10^{-15}	1.955×10^{-16}	2.0877×10^{-25}	2.431×10^{-43}	7.948×10^{-26}
n	1.7	1.867	5.5	14.75	6.896

the residual stresses (σ_x, σ_y, σ_z) along the three orthogonal directions of the specimen:

$$\sigma_i = \frac{E_{hkl}}{1 + \nu_{hkl}} \left[\varepsilon_{ii} + \frac{\nu_{hkl}}{1 - 2\nu_{hkl}} \left(\varepsilon_{xx} + \varepsilon_{yy} + \varepsilon_{zz} \right) \right] \qquad (7)$$

where E_{hkl} and ν_{hkl} are elastic modulus and Poisson's ratio. After the strain measurements, the specimen was cut by using the electro-discharge machine to prepare the 'stress free' samples, and then do value (stress free) was measured. Note that $E_{110} = 220$ GPa, $\nu_{110} = 0.28$ for FeCrAlY and $E_{111} = 205$ GPa, $\nu_{111} = 0.3$ for C276 were used.

The Si (220) bent perfect crystal was chosen for the monochromator and produced neutrons with the wavelength of 1.46 Å at the take-off angles ($2\theta_M$) of 45°. The configuration enables us to measure the (110) peak at the scattering angles ($2\theta_S$) of 41.0° for bcc FeCrAlY alloy and (111) peak at 41.0° for fcc Inconel alloy C276. Note that each peak observed at different $2\theta_S$ due to the difference in lattice spacing. The section of the gauge volume (GV) in the diffraction plane was defined by 1 mm wide cadmium slits on both incident and diffracted beams. The height of the GV was also defined by the 1 mm height of the incident beam. Thus, the GV was $\sim 1 \times 1 \times 1$ mm^3 for the three orthogonal directions of the specimen. Eight points (± 3, ± 2, ± 1, ± 0.1 form the mid-thickness), through thickness were measured, as marked in Fig. 5(a). Owing the mixture of the two phases near the mid-thickness (0 mm) the diffraction peak is weak and the error bar of the stress is relatively larger than elsewhere.

Stress components from FE analysis are obtained in the following direction: (1) transverse stress S11, representing the stress in X-axis direction, (2) stress S22, referring to the stress in Y-axis direction, and (3) stress S33 is the stress in Z-axis direction.

Fig. 6 shows residual stress distribution by simulation and experimental. Overall it shows a good trend between the simulation and neutron diffraction measurements. Specifically, the ND results show that the tensile of ~ 200 MPa in the FeCrAlY part turns to compression of approximately -200 MPa in the C276 part of the specimen. In some measure points, there is a discrepancy between FEM and ND. It could be due to the uncertainties in the measurement of stress free state in ND. As shown for this sample, it is very difficult to measure because the plate is a dissimilar weld and their chemical compositions can be mixed due to the element diffusion at high temperature brazing. Another reason can be attributed to, the initial plate states, which may contain as-fabricated residual stresses and those have not been considered in this calculation. The comparison of results obtained from ND and FEM proves that the present complex model and FEM calculation are convincing. It should thus be reasonable to extend the current approach to simulate the residual stress of the bonded compliant seal structure.

4. Results and discussion

4.1. Effect of temperature distribution

Fig. 7 shows the temperature fields for the three FE models of different meshes at 170 min in stage (5) (as shown in Fig. 3). Fig. 8
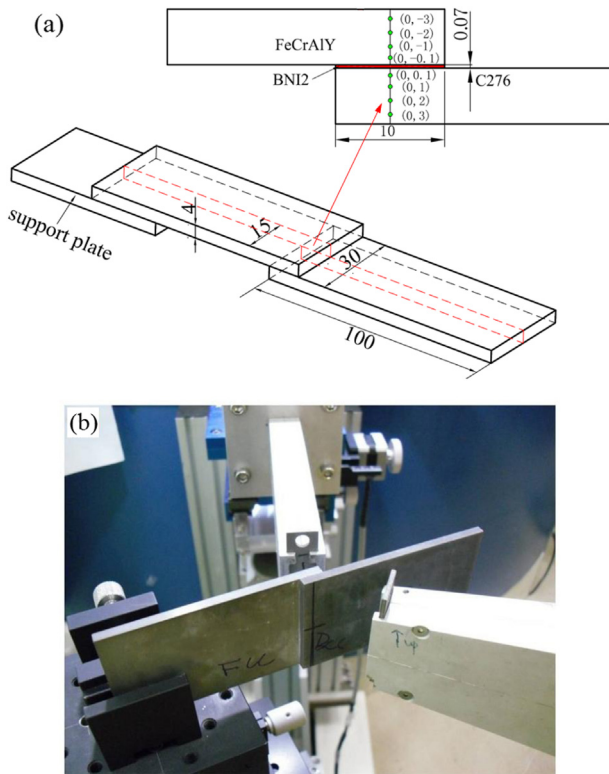
(a)

(b)

Fig. 5. Sketching of the simplified verification model (a) and sample mounting for measurement (b).

shows the node temperature varying with the time at location A in Fig. 7. It is seen that the temperature fields and node temperature varying with the time are nearly the same, indicating that the used mesh sizes are appropriate to guarantee the calculation precision. The contour of the temperature field shows that there exists a temperature gradient through the structure. The temperature distribution, however, was assumed uniform by using the previous simplified method [9–12]. In this study, the effect of the temperature gradient on residual stress is considered, in order to get a more reliable result.

For comparison, the residual stress is also calculated by the simplified method [9–12]. Table 4 lists the maximum residual
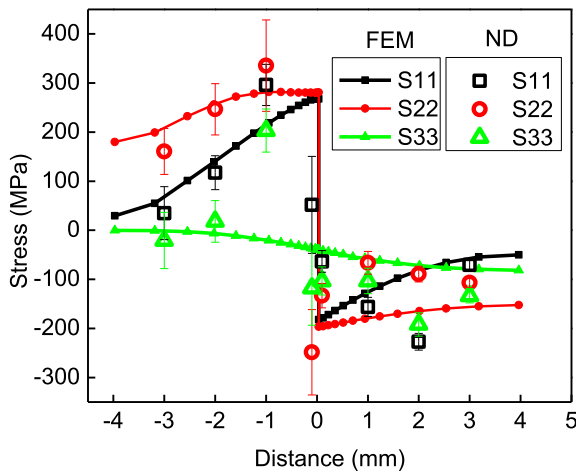

Fig. 6. Residual stress by simulation and neutron diffraction measurement for the verification model.
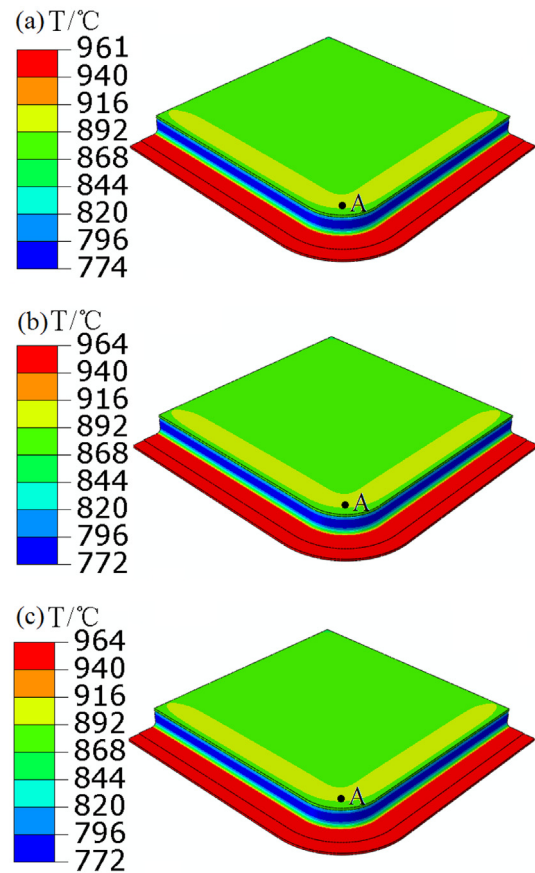
(a) T/°C

(b) T/°C

(c) T/°C

Fig. 7. Temperature field: model with element number of 40318 (a), 66798 (b) and 81102 (c).

stresses obtained by the two methods. It obviously shows that the results are different, especially in the foil and frame. The maximum S11 in the foil and frame by the simplified method and the present method are 377.4 MPa and 103.3 MPa, 400.2 MPa and 112.7 MPa, respectively. As the simplified method does not consider the temperature gradient effect, it hence underestimates the result. It should be noted that the magnitudes of S11 and S22 are equal, but the stress distributions are different, as shown in Fig. 9. This is due to that the BCS structure is geometrically symmetrical, S11 in the X-
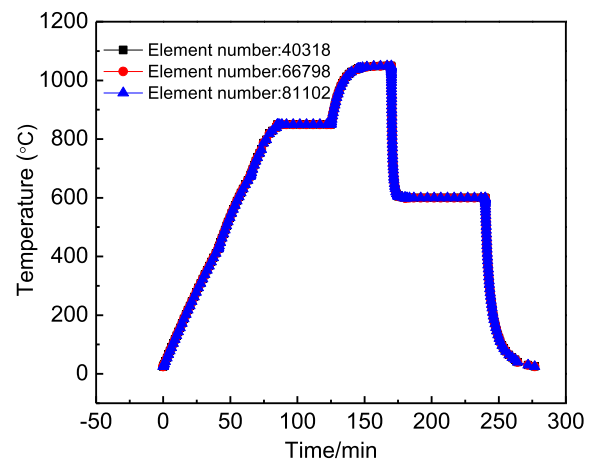

Fig. 8. Temperature varies with the time in location A in Fig. 1 with different element numbers.

Table 4
Maximum residual stresses in BCS structure with different model.

Calculation method	Maximum stress	Cell (MPa)	Ag–CuO (MPa)	Foil (MPa)	BNi-2 (MPa)	Frame (MPa)
Simplified method	S11	81.46	236.2	377.4	360	103.3
	S22	81.46	236.2	377.4	360	103.3
	S33	40.72	26.87	322	41.01	18.89
Present method	S11	80.97	232.9	400.2	366.5	112.7
	S22	80.97	232.9	400.2	366.5	112.7
	S33	40.30	27.81	304	44.66	20.17

direction is the same as S22 in the Y-direction, and S11 in the y-direction is the same as S22 in the X-direction. For this reason, S22 will not be considered in the following discussion. Because the component thickness is very small (Z-axis direction), S33 is also very small and has thus not been discussed in the following sections.

4.2. Effect of creep relaxation

Table 5 lists the maximum S11 changing with holding time. As the holding time increases to 80 h, the maximum residual stresses in cell and foil decrease from 80.97 MPa to 400.2 MPa and 60.85 MPa to 366.4 MPa, respectively, while the stresses in Ag–CuO, BNi-2 and frame change lightly. This indicates that the stresses in cell and foil produced in the cooling process have not reached the yield stress, so the creep occurring in the holding time has a positive effect on the relaxation of residual stress, while the stresses in Ag–CuO, BNi-2 and frame have already approached or exceeded the yield strength. As listed in Table 5, when the holding time exceeds 40 h, the stresses in cell and foil are also kept almost unchanged. This suggests that creep has little effect on the maximum stress from then on.

In order to determine the optimum holding time, we make a further investigation to study the creep relaxation effect on the residual stresses in each component with the time increasing.

Fig. 10 shows S11 along path P1 in cell at different holding times. It confirms that the residual stresses decrease obviously in location

Fig. 9. Residual stress contours of S11 (a) and S22 (b) in the foil.

AB with the holding time increasing, while the stresses in location BD change little. The residual stresses in location AB are reduced from −165 MPa to −120 MPa with the holding time up to 60 h. Since the geometry of BCS structure is symmetric, the magnitude and variation of S22 in location CD are the same as the S11 in location AB. From the above analysis it concludes that the creep has a large influence on the residual stress in cell. When the holding time increases from 40 h to 60 h, the stress in location AB only decrease to 2 MPa, showing that the creep has little effect on the residual stress in cell in this stage.

Described in Fig. 11 are the residual stresses along the center of Ag–CuO at different holding times. The stress distribution is similar with that in cell. In the area of EF, the stresses decrease from 174 MPa to 152 MPa with the holding time up to 60 h. In the vicinity of location G, the residual stress reaches the maximum value, and then decreases slightly in GH. A strange phenomenon is that the residual stresses in EF are relatively smaller than those in GH. This is because the relative position of location AB in Fig. 10 and EF in Fig. 11 are the same, and the changes are corresponded with each other. Similar to the situation in cell, the residual stresses in Ag–CuO have no obvious change when the holding time exceeds 40 h.

Fig. 12 shows the residual stresses along path P2 at different holding times. The residual stress in the region of Ag–CuO joint is tensile and is greatly influenced by the creep effect. In BNi-2 joint the stress is compressive and decreases slightly. In the middle of the path P2, there is a large stress gradient which is mainly caused by the deformation of the other components in BCS structure. The foil absorbs the stresses of the adjacent components by the elastic and plastic deformations of itself to decrease the stresses in the whole structure.

Fig. 13 depicts the residual stresses along the center of BNi-2 at different holding times. It shows that in the first part of the path, the residual stress decreases greatly at first and then become insensitive to the creep effect. For the rest of the path, the residual stresses change slightly with the increasing of holding times, and there is the same tendency as that in the center of frame (see Fig. 14). This is because the stress in BNi-2 has reached the yield state, and the creep has little effect on the residual stress. As the BNi-2 and frame are mutually constrained with each other, the stress in frame reveals a similar tendency.

From the above analysis we conclude that in the region of Ag–CuO joint, the residual stresses have been influenced dramatically by the creep effect, while in the area of BNi-2 joint the stresses have been affected slightly. Since the material of cell is ceramic and yield phenomenon does not exist, the stress in the cell influences all the stresses in the region of Ag–CuO. In the location of BNi-2 joint, all the materials can undergo yield, and the stresses produced in this area are large enough to approach or even exceed the yield state. Therefore, the effect of creep in this region has little impact on the residual stress.

Due to the creep effect, the maximum residual stresses in the cell and foil have been decreased about 23% and 8.3%, respectively,
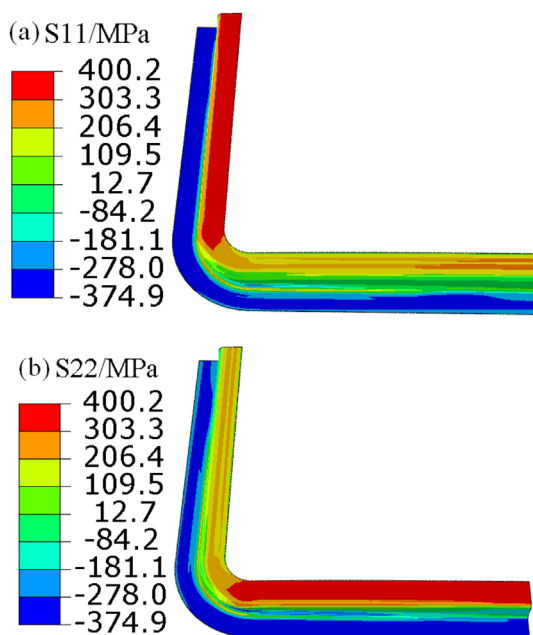
Table 5
Maximum residual stresses S11 in BCS structure.

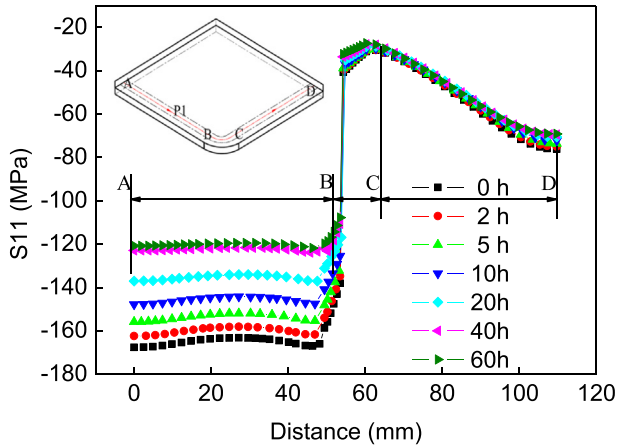| Holding time (h)	Cell (MPa)	Ag–CuO (MPa)	Foil (MPa)	BNi-2 (MPa)	Frame (MPa)
0	80.97	232.9	400.2	366.5	112.7
2	78.85	232.4	400.2	366.4	112.3
5	76.13	231.8	400.2	366.3	111.9
10	72.60	230.9	390.4	366.1	111.2
20	67.64	230.6	380.1	365.9	110.3
40	62.37	230.5	366.9	365.4	109.1
60	61.57	229.2	366.4	365	108.3
80	60.85	229.2	366.4	364.7	107.7

Fig. 10. Effect of holding time on residual stress in cell.
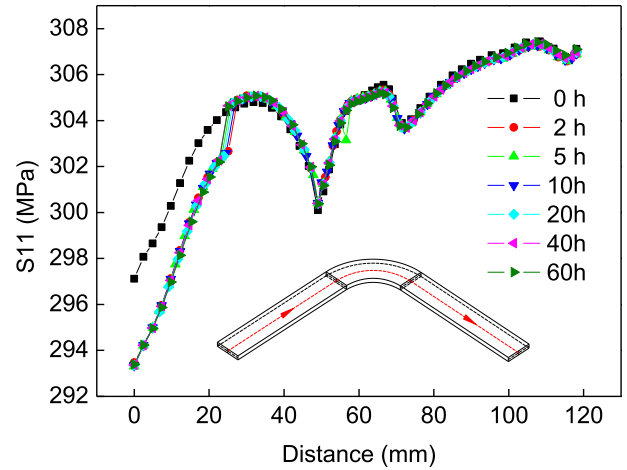

Fig. 13. Effect of holding time on S11 in BNi-2.
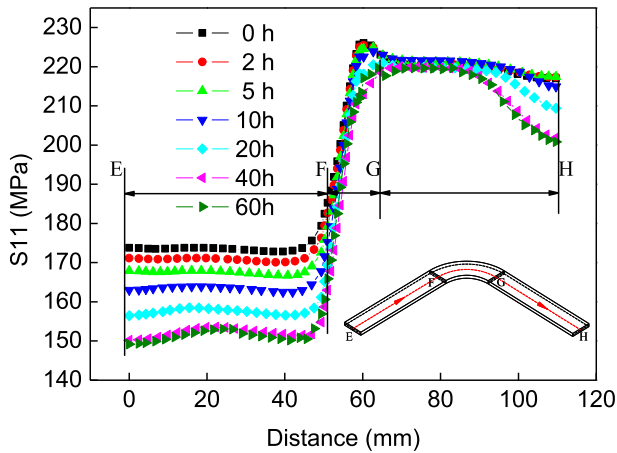

Fig. 11. Effect of holding time on S11 in Ag–CuO.
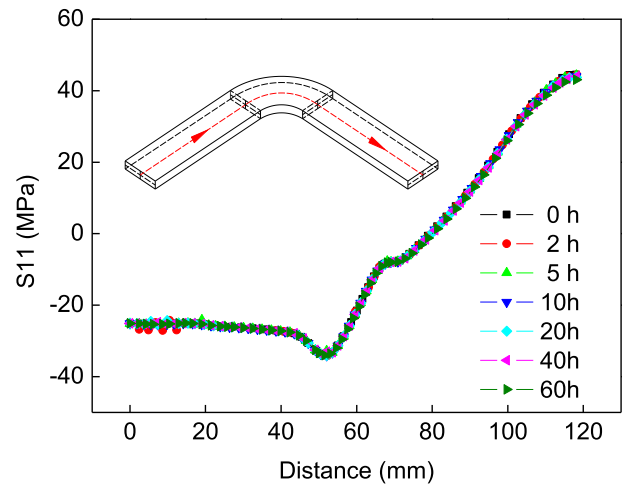

Fig. 14. Effect of holding time on S11 in frame.

as the holding time at 600 °C increases up to 40 h. The residual stresses in cell, Ag–CuO and foil located in the region of the multi-layer structure have been reduced about 26.9%, 13.6% and 22.1%, which cause a corresponding reduction of minimum creep rate about 40%, 23.9% and 69.2% estimated by Eq. (4) and material constants in Table 3, respectively. It is obvious that the creep relaxation greatly reduces the risk of creep failure at high temperature.
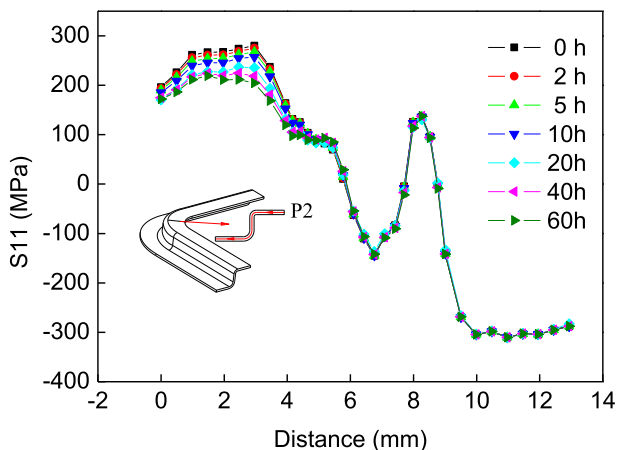
5. Conclusions

This paper presents a discussion on how to decrease the residual stress by using short-time creep relaxation effect in the BCS structure of a planar SOFC. Based on the simulated results by finite element method, the following conclusions can be obtained.

(1) The previous simplified modeling underestimates the residual stress, because the temperature gradient within structure induced by the heat conduction, convection and radiation was not taken into account

(2) It is proved that the residual stress can be decreased greatly by making use of the short-time creep relaxation effect. By designing a holding time at 600 °C for 40 h, the maximum residual stresses in cell and foil have been decreased by 23% and 8.3%, respectively, while the stresses in Ag–CuO, BNi-2 and frame are changed slightly. When the creep time exceeds 40 h, the residual stresses in all the components change slightly.

(3) The residual stresses in cell, Ag–CuO and foil located in the cell-to-foil joint have been decreased by 26.9%, 13.6% and 22.1%, which may result in a corresponding reduction of minimum creep rate of about 40%, 23.9% and 69.2% at high temperature, respectively. Considering the stress

Fig. 12. Effect of holding time on S11 in foil.

redistribution in the whole structure, it is suggested that the holding time exceeding 40 h be unnecessary in the present case and it should be determined case by case to consider the influence of geometry, materials, and brazing process.

Acknowledgments

References

[1] Xiang Zhao, Fenghui Wang, Jianye Hang, Tiejun Liu, J. Power Sources 201 (1) (2012) 231–235.
[2] H. Yakabe, T. Ogiwara, M. Hishinuma, I. Yasuda, J. Power Sources 102 (1–2) (2001) 144–154.
[3] Sea-Fue Wang, Yuh-Ruey Wang, Yung-Fu Hsu, Ching-Chin Chuang, Int. J. Hydrogen Energy 34 (19) (2009) 8235–8244.
[4] Julie Villanova, Olivier Sicardy, Roland Fortunier, Jean-Sébastien Micha, Pierre Bleuet, Nucl. Instrum. Methods Phys. Res. B 268 (3–4) (2010) 282–286.
[5] Shiru Le, Zhemin Shen, Xiaodong Zhu, et al., J. Alloys Compd. 496 (1–2) (2010) 96–99.
[6] K.S. Weil, J.S. Hardy, B.J. Koeppel, J. Mater. Eng. Perform. 15 (4) (2006) 427–432.
[7] K.S. Weil, B.J. Koeppel, J. Power Sources 180 (1) (2008) 343–353.
[8] Arata Nakajo, Christoph Stiller, Gunnar Harkegard, Olav Bolland, J. Power Sources 158 (1) (2006) 287–294.
[9] K.S. Weil, B.J. Koeppel, Int. J. Hydrogen Energy 33 (14) (2008) 3976–3990.
[10] Wenchun Jiang, Shan-Tung Tu, Guocheng Li, Jianming Gong, J. Power Sources 195 (11) (2010) 3513–3522.
[11] Wenchun Jiang, Yucai Zhang, Wanchuck Woo, Shan-Tung Tu, J. Power Sources 196 (24) (2011) 10616–10624.
[12] Wen-chun Jiang, Yucai Zhang, Wanchuck Woo, Shan-Tung Tu, J. Power Sources 209 (1) (2012) 65–71.
[13] Wenchun Jiang, Jianming Gong, S.T. Tu, Mater. Des. 31 (1) (2010) 648–653.
[14] Wenchun Jiang, Jianming Gong, Shan-Tung Tu, Mater. Des. 31 (4) (2010) 2157–2162.
[15] Liyan Qin, Shoulu Zhang, Shizhe Song, J. Chin. Soc. Corros. Prot. 26 (1) (2006) 1–5.
[16] Tsung Leo Jiang, Ming-Hong Chen, Int. J. Hydrogen Energy 34 (19) (2009) 8223–8234.
[17] Lieh-Kwang Chiang, Hui-Chung Liu, Yao-Hua Shiu, Chien-Hsiung Lee, Ryey-Yi Lee, Renew. Energy 33 (12) (2008) 2580–2588.
[18] Chih-Kuang Lin, Tsung-Ting Chen, Yau-Pin Chyou, Lieh-Kwang Chiang, J. Power Sources 164 (1) (2007) 238–251.
[19] http://www.matweb.com.
[20] Giuliano Gregori, Lí Lì, John A. Nychka, David R. Clarke, Mater. Sci. Eng. A 466 (1–2) (2007) 256–264.
[21] M.L. Hattali, S. Valette, F. Ropital, N. Mesrati, D. Tréheux, J. Mater. Sci. 44 (12) (2009) 3198–3210.
[22] Shiva Gadag, Ganesh Subbarayan, J. Mater. Sci. 41 (4) (2006) 1221–1232.
[23] Frederick Harwood Norton, McGraw-Hill book company, New York, 1929.
[24] O. Golan, A. Arbel, D. Eliezer, D. Moreno, Mater. Sci. Eng. A 216 (1–2) (1996) 125–130.
[25] Z.F. Yue, G. Eggeler, B. Stöckhert, Comp. Mater. Sci. 21 (1) (2001) 37–56.
[26] J. Laurencin, G. Delette, F. Usseglio-Viretta, S. Di Iorio, J. Eur. Ceram. Soc. 31 (9) (2011) 1741–1752.
[27] S.J. Bull, Oxid. Metals 49 (1998) 1–17.
[28] Wenchun Jiang, Jianming Gong, Hu Chen, Shan-Tung Tu, Int. J. PVP 85 (8) (2008) 569–574.
[29] Mansur Akbari, Sebastian Buhl, Christian Leinenbach, Ralph Spolenak, Konrad Wegener, Mech. Mater. 52 (1) (2012) 69–77.
[30] Jinjiang Yu, Xiaofeng Sun, Tao Jin, Z. Nairen hao, Hengrong Guan, Zhuangqi Hu, Mat. Sci. Eng. A 527 (9) (2010) 2379–2389.
[31] Raymond R. Unocic, Ph.D. Thesis, The Ohio State University, Ohio, USA (2008).
[32] Wanchuck Woo, Vyacheslav Em, Pavel Mikula, Gyu-Baek An, Baek-Seok Seong, Mater. Sci. Eng. A 528 (12) (2011) 4120–4124.